Insertion of fluorine into a LiFePO 4 electrode material by gas–solid fluorination

Lemoine Kevin, Kenmogne-Debah Roméo, Doubtsof Léa, Frezet Lawrence, Petit Elodie, Guerin Katia, Bertrand Devouard, Sougrati Moulay-Tahar, Delbègue Diane, Bonnet Pierre

Insertion of fluorine in $LiFePO_4$ electrode material by gas-solid fluorination

Lemoine Kevin*[a] , Kenmogne-Debah Roméo[a], Doubtsof Léa[a], Frezet Lawrence[a], Petit Elodie [a], Guerin Katia [a], Devouard Bertrand [b,c], Sougrati Moulay-Tahar[d], Delbègue Diane[e] and Bonnet Pierre*[a]

[a]*Université Clermont Auvergne, CNRS, ICCF, 24, Avenue Blaise Pascal, 63178 Aubière, France.*

[b]*Laboratoire Magmas et Volcans, CNRS UMR 6524, Université Clermont Auvergne, IRD, OPGC, 63170 Aubière, France.*

[c]*CEREGE, Aix Marseille Univ, CNRS, IRD, INRAE, 13545 Aix-en-Provence, France.*

[d]*ICGM, University of Montpellier, CNRS, ENSCM, Montpellier, France.*

[e]*Centre National des Etudes Spatiales, 18 avenue Edouard Belin 31 401 Toulouse Cedex 9, France.*

*corresponding authors :

Lemoine Kevin : kevin.lemoine@uca.fr

Bonnet Pierre : pierre.m.bonnet@uca.fr

Keywords: Fluorination, solid/gas reaction, iron-based materials, secondary batteries.

Abstract: In this study, the insertion of fluorine in $LiFePO_4$ was carried under molecular fluorine F_2 at different temperatures. The reactivity strongly depends on the applied fluorination temperature leading to very different products: a core delithiation of the material is observed at low temperatures with the formation of a LiF shell around the particles, while the material decomposes to gradually form a mixture of α-FeF_3 and α-Li_3FeF_6 iron fluorides at higher temperatures. A second thermal treatment under N_2 leads to the formation of $LiFePO_4F$ according to a new way not yet reported. Supported by X-Ray Diffraction, Raman, infrared and Mössbauer spectroscopies, ^{7}Li Nuclear Magnetic Resonance, and electrochemical characterizations of the different materials, this overall view demonstrates the various fluorination mechanisms for $LiFePO_4$, from the chemical delithiation to then stabilize the pure fluorinated form $LiFePO_4F$ or illustrates an innovative way that could be extendable to obtain the triphylite form of $NaFePO_4$.

1 Introduction

With the average energy needs of each individual growing over the past two decades, the improvement of the energy storage such as the lithium-ion batteries (LIBs) is a major challenge.[1–3] Also, the lithium cobalt oxide employed as the positive electrode in Li-ion batteries ($LiCoO_2$ with a capacity of 150 $mAh \cdot g^{-1}$ at 3.7V) is formed with mined cobalt obtained under deplorable conditions. A non-toxic and environment friendly alternative is to look at the iron-based compounds with an abundant element in the earth's crust. But iron oxides demonstrate low potentials (~1V) and are therefore more often studied on the side of the negative electrode.[4,5] Tailoring electrodes materials by following the solid-state chemistry principles allows to modify and modulate their electrochemical

properties. Goodenough and later Tarascon et al. have well demonstrate the effect of different chemical groups nature on the material potential values.[6] For instance, the potential values are following the inductive effect of oxides lower than the corresponding phosphates, also lower than sulfates: $O^{2-} < PO_4^{3-} < SO_4^{2-}$. For that reason, $LiFePO_4$ (LFP) with the olivine crystal structure was one of the most widely used cathode materials for LIBs and is still studied nowadays.[7–9] Similarly, fluorine atom led to higher potentials than oxygen due to the larger ionicity of M–F bonds as compared to M–O bonds.[10,11] With that, inorganic fluorides such as iron fluoride FeF_3, lithiated iron fluoride like $LiFe_2F_6$ or Li_3FeF_6 were studied as potential positive electrode candidates.[12–16] Li_2FePO_4F and $LiFePO_4F$ fluorophosphates, $LiFeSO_4F$ fluorosulfate, among others, were investigated to be possible iron-based target solutions for the positive side of secondary batteries and are the subject of numerous studies offering a strong framework acting as host for Na or Li insertion.[17–22] As a result, a classical picture is that the introduction of a fluorine atom in the fluorophosphate host allows to achieve high potentials, while keeping the benefit of the phosphate groups. Indeed, $LiFePO_4F$ potential value is close to the one obtained for the classic iron fluoride FeF_3 (2.8 and 3.0V, respectively), in addition to the tavorite-like structure offering a 3D network made of 1D chains of metal octahedra interconnected by phosphate tetrahedra, allowing a Li^+ diffusion compared to α-FeF_3 dense perovskite structure.[23,24] In the following, the paper is focused on the fluorination of $LiFePO_4$ iron phosphate to directly incorporate F atoms within the 3D network. Different synthesis methods for the obtention of fluorophosphate or fluorosulfate, for example, have been reported in literature such as the solvothermal or ionothermal synthesis allowing to obtain the expected phase at lower temperature unlike the classic ceramic process.[17,25,26] In this later case, the compound is directly elaborated by a stoichiometric mixture of lithium fluoride and iron phosphate (when $LiFePO_4F$ is aimed), the solid-state reaction occurs at high temperature (575°C for $LiFePO_4F$).[23,27] Generally, the ceramic method gives micrometric particles (~1 µm), while reactions in solution can lead to nanostructured materials, maximizing the specific surface for better contacts with the liquid electrolyte.[28] But at the best of our knowledge, it should be noticed that no direct gas-solid fluorination to synthesize $LiFePO_4F$ is described in the literature. The purpose of this exploratory work is the understanding of $LiFePO_4$ reactivity with gaseous fluorine (F_2), and then to illustrate the possible direct modification of this compound with the insertion of fluorine atoms in the matrix. Carefully following the characterizations of all the fluorinated phases under different conditions with Powder X-Ray Diffraction (PXRD), Raman and Mössbauer spectrometry but also gases emitted by *in situ* Fourier-transform infrared spectroscopy (FTIR), Transmission Electronic Microcopies (TEM), and ^{7}Li Nuclear Magnetic Resonance (NMR), the phases obtained were determined and the different chemical fluorination mechanisms were proposed. All the electrochemical behaviors were also investigated when used as positive electrodes for LIB with a special attention is focused on the $LiFePO_4F$ obtained compound, but also the possible cationic exchange to show an interesting way to form $NaFePO_4$ with the triphylite structure, an allotropic form only obtained with a Li/Na exchange in LiFePO4.

2 Results and discussion

2.1 Structural modifications

The $LiFePO_4$/C composite material is initially black due to the carbon coating around the grains, and its fluorination is triggering a color change, even at room temperature (Figure 1, insert). The composite was treated under molecular fluorine (F_2) in a nickel furnace under different temperatures (room temperature or RT, 125°C, 250°C, 300°C and 500°C) during 5h. For the fluorinations carried out between room temperature and 350°C, the results are quite similar, in contrast to the product obtained after fluorination at 500°C that turns out to be very different. For all PXRD patterns of materials fluorinated at temperature T < 500°C (Figure 1), the main phase can be indexed with the monoclinic anhydrous non-lithiated iron phosphate ($FePO_4$, *Pnma*[29]), a result confirmed for $LiFePO_4$-125 by Raman Spectrometry where the delithiated phase is identified in good agreement with the literature values (Figure S1).[30] The delithiation process seems to occur with the formation of LiF, with intensities of peaks at 39 and 45° for $LiFePO_4$-RT and $LiFePO_4$-125, also for $LiFePO_4$-250 and $LiFePO_4$-300 but with a decrease in intensity. Furthermore, close examination of the diffractograms shown in Figure 1 demonstrates that the Bragg peaks relative to the α-Li_3FeF_6 cryolite phase[31] (monoclinic, *C*2/*c*) start to be formed from the fluorination at 250°C, whereas they are not observed at lower temperature, thus indicating a decomposition of the initial $FePO_4$ matrix. This is induced by the departure of phosphorus atoms as highlighted on the fluorinated product at 500°C, but already beginning at 250°C even if not fully completed. For the material fluorinated at 500°C, the fluorination of the phosphate matrix is complete with Bragg peaks indexed by a mixture of iron fluorides : α-Li_3FeF_6 cryolite is formed with the lithium from $LiFePO_4$ and α-FeF_3 formation is the result of the excess of iron fluorinated after all Li^+ ions reacted.

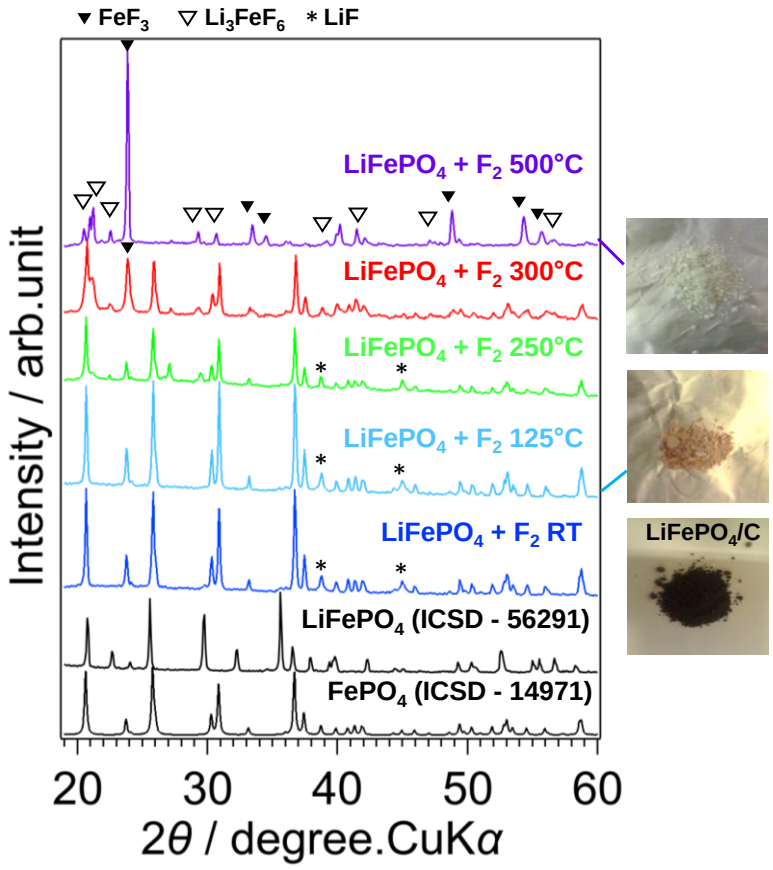

Figure 1 : Powder X-ray diffraction patterns of products obtained after fluorination at different temperatures : room temperature (RT, blue), 125 (light blue), 250 (green), 350 (red) and purple (500). Images for different materials in insert. Theoretical calculated XRD for $FePO_4$ and $LiFePO_4$ are shown in black.

For $LiFePO_4$-125, the Li^+ non-presence in the material could be elucidated with samples characterized by TEM. The starting material is coated by a carbon layer, a layer not observable anymore after fluorination at 125°C, but the formation of a new layer around the particles is observed. A chemical analysis by Energy Dispersive Spectrometry (EDS) was performed on the particles core and no fluorine atoms are significantly detected, resulting in an atomic composition close to $FePO_4$ (Figure S2). The TEM images show particles surrounded by a layer made of dendrites (Figure 2, left). Their chemical analysis mostly shows a fluorine rich area leading to the conclusion that fluorine is here combined with a very light element not measurable by EDS, in our case Li (Figure S3). This hypothesis is well consistent with the diffuse electron diffraction patterns obtained by selected area electronic diffraction on this layer (insert in Figure 2, left) showing distinct diffraction fringes which are in good concordance with the LiF structure, also confirmed by ^{7}Li NMR with a spectrum with spinning sidebands, and its isotropic position at -1.4 ppm, all similar to LiF. The ^{7}Li NMR peaks are broader compared to the classic signature for LiF, indicating an important coupling between Li and Fe atoms in $FePO_4$, known to be paramagnetic, and confirms that $FePO_4$ particles are intimately coated by

LiF layers (Figure 2, right), a phenomenon observed already in metal oxides coated by LiF.[32] All these indications lead to conclude that after fluorination at low temperature, T < 250°C, the material is organized in a core shell type structure: a delithiated iron phosphate in the centre surrounded by a LiF coating layer.

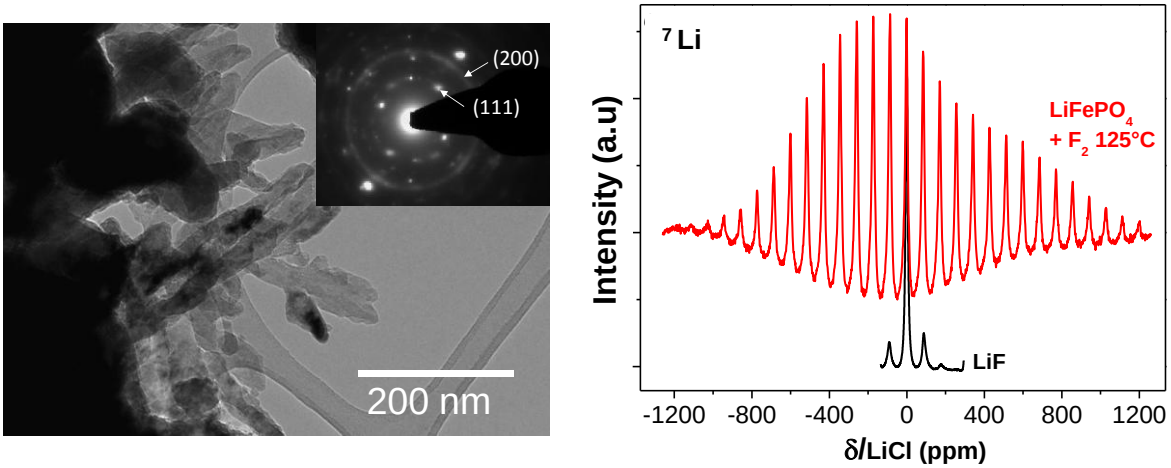

Figure 2 : TEM images (left) and ^{7}Li NMR spectra of $LiFePO_4$ + F_2 125°C (right).

During the fluorination, the gases emitted are collected and analyzed by *in situ* FTIR. As can be seen on the spectra presented in Figure 3, between 250°C and 500°C, the presence of PO_3F molecules is observed with broad peaks around 990 cm^{-1} and 1420 cm^{-1}, and around 1030 cm^{-1} for PF_5. During the fluorination, the initial carbon layer, reducing phosphate grains, is also consumed with the formation of volatile species such as CF_4 or C_2F_6 (Figure 3).

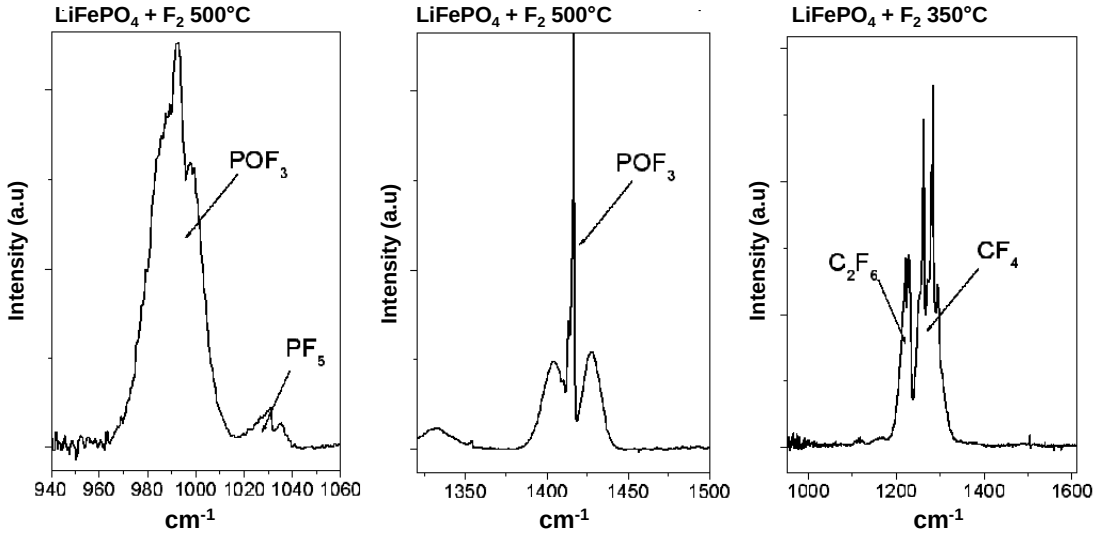

Figure 3 : Infrared spectra of emitted gas during the fluorination of $LiFePO_4$ up to 500°C.

To fully confirm the thermal behavior with the fluorination, measurements by Mössbauer spectrometry were carried out. The spectra are shown in Figure 4 and were fitted with the hyperfine

parameters reported in Table 1. The spectrum and parameters of the initial material are in perfect agreement with those given in the literature for the $LiFePO_4$ phase.[33] For fluorinated materials, it is noticeable that at room temperature the hyperfine parameters obtained can be assigned to a typical $FePO_4$ signature, in good agreement with previous XRD and Raman results, and up to 350°C. However, a second paramagnetic contribution (δ = 0.38 and ΔE_Q = 0.36 $mm.s^{-1}$) increases gradually with higher fluorination temperature. This contribution is in good agreement with α-Li_3FeF_6 hyperfine values, even compared with the spectra obtained from α-Li_3FeF_6 synthesized at high temperature by a stoichiometric mixture of LiF and α-FeF_3 (Figure S4). Finally, for the fluorinated material at 500°C, the Mössbauer spectrum can be fitted with two contributions: a paramagnetic doublet (δ = 0.43 and ΔE_Q = 0.36 $mm.s^{-1}$) corresponding to α-Li_3FeF_6 as well as a magnetic sextet (δ = 0.43 and 2ε = 0.36 $mm.s^{-1}$, H = 40 T) for α-FeF_3.[34] Those two contributions are in perfect agreement with the XRD assignments made on this compound.

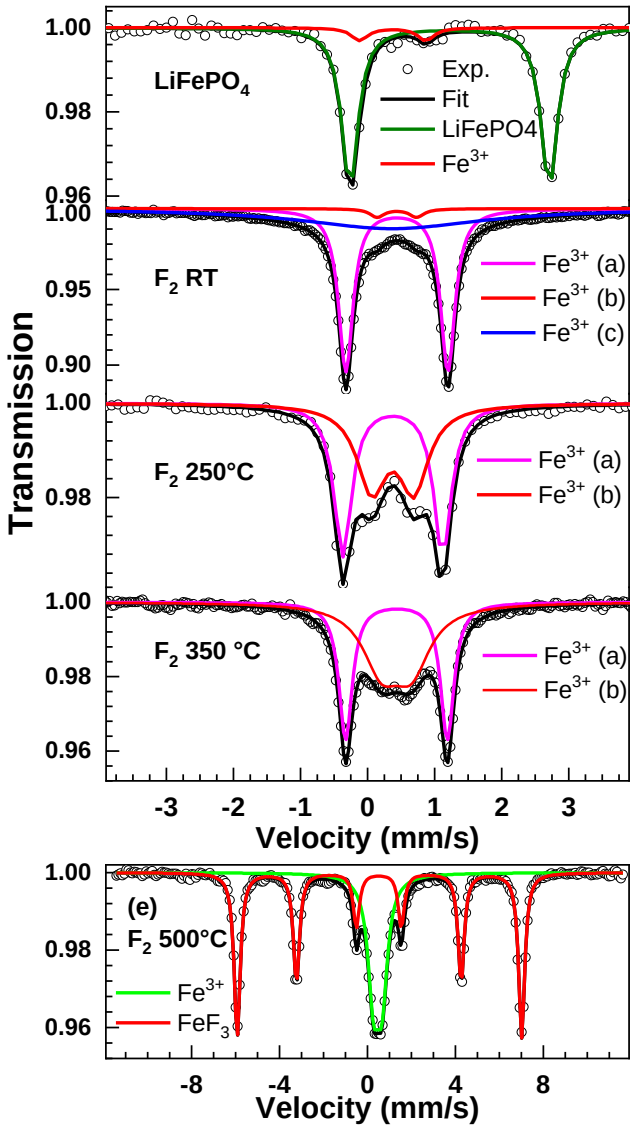

Figure 4 : ^{57}Fe Mössbauer spectra at 300 K of $LiFePO_4$ and fluorinated materials (see Table 1).

Thus, the XRD-Mössbauer cross-analysis clearly shows that the fluorination mechanism of $LiFePO_4$ seems to take place in two stages: the chemical delithiation followed by the collapsing of the phosphate structure. The complete chemical disinsertion of the Li atoms by fluorine is a favored process even at room temperature ($\Delta_r G°$=-612,1 kJ/mol), possible because of the robustness of the phosphate network not changing during this process and also not causing any irreversible change within the material structure. Over the past several years, different models have been proposed to describe the Li^+ movement and phase transformations in $LiFePO_4$, resulting in a the two-phase insertion/extraction mechanism in $LiFePO_4$ happening simultaneously with the oxidation of Fe^{2+} to Fe^{3+}.[19] In the second step, with temperatures higher than 250°C, the fluorination of $FePO_4$ cores leads to the formation of POF_3 and PF_5 gases and the fluorination of iron atoms into α-FeF_3. From 250°C, under the action of temperature, α-FeF_3 reacts with LiF to give α-Li_3FeF_6. Beyond 350°C, the destruction of the phosphate network is complete giving a mixture of α-FeF_3 and α-Li_3FeF_6. It should be noted that in this scenario, the final FeF_3 is therefore the excess unreacted with LiF.

Table 1 : Refined values at 300 K for $LiFePO_4$ and the different fluorinated materials.

	Fe^{n+}	δ	$\Delta E_Q/2\varepsilon$	τ
$LiFePO_4$				
2 quadrupolar components	Fe^{2+}	1.22	2.97	0.93
	Fe^{3+}	0.37	0.99	0.07
$LiFePO_4$ + F_2 RT				
3 quadrupolar components	Fe^{3+} (a)	0.44	1.52	0.55
	Fe^{3+} (b)	0.44	0.59	0.03
	Fe^{3+} (c)	0.37	0.00	0.42*
$LiFePO_4$ + F_2 250				
2 quadrupolar components	Fe^{3+} (a)	0.38	1.49	0.52
	Fe^{3+} (b)	0.38	0.63	0.48
$LiFePO_4$ + F_2 350				
2 quadrupolar components	Fe^{3+} (a)	0.43	1.52	0.45
	Fe^{3+} (b)	0.43	0.45	0.55
$LiFePO_4$ + F_2 500				
2 quadrupolar components	Fe^{3+}	0.47	0.39	0.38
	Fe^{3+}	0.53	0.03	0.62**

*Fe^{3+} in small particles (nano effect) resulting in a large continuous background ;**α-FeF_3 with a hyperfine field H = 40 T.

Two hypotheses are possible about the obtained composition of the material: 1/ a mixture of neighboring α-Li_3FeF_6 and α-FeF_3 particles or 2/ a core-shell like structure with a α-Li_3FeF_6 shell

around α-FeF_3, after reaction of the external α-FeF_3 with a LiF coating. Because of the sensitivity of α-Li_3FeF_6 under the high energy electron beam, the TEM analysis does not allow to give the information by diffraction, but the chemical analysis of the material obtained with the fluorination at 350°C showed no trace of fluorine in the grain center, only at the periphery. In parallel, previous characterizations clearly indicated that a significant amount of Li_3FeF_6 is formed at this temperature. If scenario 1/ is correct, many grains with fluorine in the center of the particle should be found, which is not the case. This concludes that fluorine converts first outside of $FePO_4$ particles into FeF_3 which immediately reacts with LiF to give Li_3FeF_6. Then when all the LiF around the grain has been consumed, the core of the grain, $FePO_4$, is then converted to FeF_3. These results suggest a final structure with a α-FeF_3 core and a α-Li_3FeF_6 shell, in good agreement with the hypothesis 2/.

2.2 Synthesis of $LiFePO_4F$

After the fluorination of $LiFePO_4$ at 125°C, it was shown that an intimate mixture of LiF and $FePO_4$ was obtained, a mixture generally used to synthesize $LiFePO_4F$ by the classic ceramic method. To follow this idea, an annealing treatment of the LiFePO4 + F_2 125°C mixture under unreactive gas (N_2) is done at 550°C during 24h. The product obtained by this treatment is further noted $LiFePO_4$ -125 + N_2. The XRD pattern of the annealed product is corresponding to $LiFePO_4F$ Brag peaks confirming the total reaction of $FePO_4$ (Figure 5, left) with TEM photograph in insert showing that the prepared material is formed by individual sub-micronic particles (~500-1000 nm), without carbon layer, in good concordance with the classical solid-state method. This result is also confirmed by Mössbauer Spectrometry with a sharp quadripolar doublet observed at 300 K that can be described by a unique component corresponding to Fe^{3+} in $LiFePO_4F$ (δ = 0.44 and ΔE_Q = 1.13 $mm.s^{-1}$). Infrared spectroscopy proves the absence of hydroxide groups, totally ruling out the possibility of having formed the $LiFePO_4(OH)$ form of similar structure (Figure S5). Thus, the gas-solid fluorination of $LiFePO_4$ appears as a new and original method of synthesis of $LiFePO_4F$.

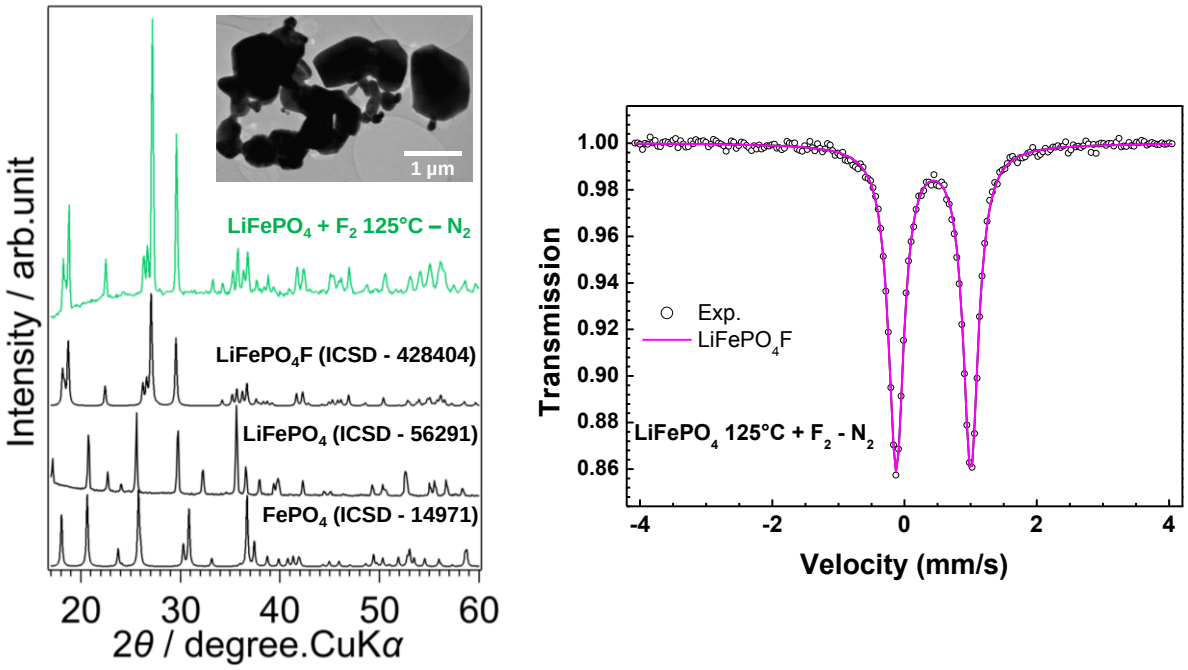

Figure 5 : XRD pattern, MET image in insert (left), and Mössbauer spectrum at 300 K (right) of $LiFePO_4 + F_2$ 125°C – N_2.

To extend the study, similar treatment has been done with $LiFePO_4$ fluorinated at room temperature ($LiFePO_4$ – RT) which could result in already carbon coated $LiFePO_4F$, a favourable aspect when the electrochemical application is aimed. In XRD pattern of the obtained product (noted $LiFePO_4$ - RT + N_2), all peaks can be attributed to a mixture of $LiFePO_4$ (triphylite) and $LiFePO_4F$. Unlike the fluorinations at higher temperatures, the particles of $LiFePO_4$–RT are still coated by carbon which reduces a part of iron and can induce a partial defluorination of $LiFePO_4F$ during the thermal treatment under N_2. As a consequence, this indicates that no carbon coated $LiFePO_4F$ particles can be obtained by this way, moreover it shows that no $LiFe^{2+}_{(1-x)}Fe^{3+}_xPO_4F_x$ compounds are observed.

2.3 Electrochemical study

The galvanostatic curves after 5 cycles for the samples $LiFePO_4 + F_2$ – 250°C and 500°C are shown in Figure 6. Those results are compared these to $LiFePO_4F$ synthesized after the annealing under N_2. The galvanostatic profile of $LiFePO_4F$ (Figure 6, left) is similar to the one of $LiFePO_4 + F_2$ – 250°C and classical of a lithium insertion process with a flat plateau both in oxidation and reduction. The case of $LiFePO_4 + F_2$ – 500°C is totally different with a huge polarization in between oxidation and reduction a classical process of a structural conversion during electrochemistry. The highest potential of use (3.3V) but also the lowest capacity (45 $mAh.g^{-1}$) is obtained for $LiFePO_4 + F_2$ – 250°C. 0.26 Li^+ are inserted for a cut off voltage in discharge of 2.8V. The discharge cut off voltage may be a bit high but, as no more capacity is reached below 2.8V, it was chosen to avoid any conversion mechanism. The potential is in good agreement with previous studies, whereas the capacity reached is quite lower than expected (C_{th} = 178 $mAh.g^{-1}$).[20] Furthermore, the LiF layer around the $FePO_4$ particles could also

explained the lack of lithium diffusion. A small plateau during the reduction process is also observable, around 3.2V, and can be explained by the potential of insertion for α-Li_3FeF_6 particles, as their formation was shown with the XRD and the Mössbauer spectrometry analysis. With the post-treatment under nitrogen ($LiFePO_4$ - 125 + N_2 or $LiFePO_4F$), the potential obtained is 2.7V with a higher capacity up to 55 $mAh.g^{-1}$ corresponding to 0.34 Li^+ inserted. As a comparison, a maximum insertion of 0.4 Li^+ has been obtained for $LiFePO_4F$ from an ionothermal synthesis.[35] For higher potential than 2.7V and 0.2 Li^+, Chen et al. have suggested that the electrochemical process was typical of a single-phase process whereas for lower potential, a two-phase lithium intercalation occurs.[20] Our synthesis conditions could prevent from the two phases lithium intercalation process with the increase of the particle size. Similar effect of high polarization coupled to a low capacity was noticed by Ellis et al. for as-prepared $LiFePO_4F$ having large particle size which are not carbon coated.[25] This polarization still increases with the increase of fluorination temperature (500°C) not mainly because of the increase of the particle size but because of a new electrochemical process: the conversion reaction of the mixture FeF_3/Li_3FeF_6. Both phases are electrochemical active and leads to iron metal at the lower reduction state with a 3 electrons process but with a high voltage hysteresis. An intermediate insertion process occurs for both FeF_3 and Li_3FeF_6 in between 3.5 and 1.2V leading to $Li_{0.5}FeF_3$ and Li_4FeF_6.[15,36] A capacity of about 40 $mAh.g^{-1}$ is associated to this phenomenon. Fe^{2+} are then converted into Fe^0 with a capacity of 199 $mAh.g^{-1}$. It is possible to compare this value to the theoretical one of 522 $mAh.g^{-1}$ which results from 2/3 of the theoretical value of FeF_3 (714 $mAh.g^{-1}$) and 1/3 of the one of Li_3FeF_6 (140 $mAh.g^{-1}$). The possible core-shell structure could explain the low capacity obtained for this mixture of fluorinated material at 500°C, with the core FeF_3 only reacting after the Li_3FeF_6 shell.

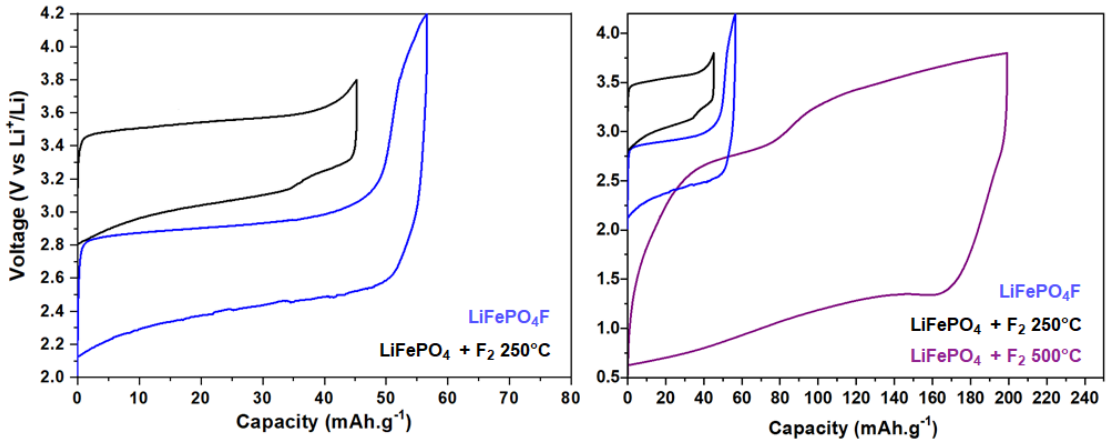

Figure 6 : Charge/discharge curves for the fifth cycle of $LiFePO_4$ + F_2 250°C between 3.8 - 2V and $LiFePO_4F$ between 4.2 – 2.1V (left), and $LiFePO_4$ + F_2 500°C between 3.8 - 0.7V (right).

A second test was inspired by the different chemical Li/Na ions exchanges in $LiFePO_4$ with the triphylite structure, keeping this thermodynamically unstable structure for $NaFePO_4$, whereas

$NaFePO_4$ is obtained with the maricite structure when synthesized classically.[37–39] It should be noted that the lithium deinsertion was chemically possible with different techniques such as the use of Br_2 or Cl_2.[40,41]With the obtention of the $FePO_4$ phase for $LiFePO_4$ - RT, this material was rinsed with electrolyte solvent to remove the LiF shell. Then, the material was tested with sodium metal as an anode. The galvanostatic curves are shown in Figure. The material is electroactive with a plateau 0.3V below $LiFePO_4$ as expected versus Na^+/Na. The capacity obtained is ~130 $mAh.g^{-1}$ up to 4 cycles (Figure 7), a bit lower than the theoretical one (C_{th}=154 $mAh.g^{-1}$), a result that could be explained by some residual lithium within the phosphate structure. Further fluorination in time and at a slightly higher temperature should reduce this lithium residue.

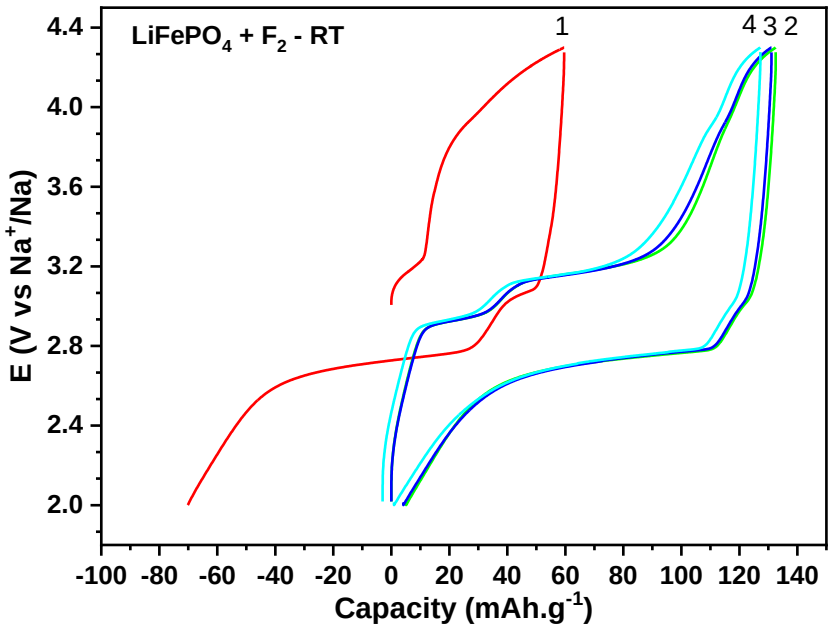

Figure 7 : Charge/discharge curves for the first 4 cycles of $LiFePO_4 + F_2$ - RT between 4.2 - 2V with a sodium anode.

3. Conclusion

In this study of fluorination of $LiFePO_4$ by molecular fluorine F_2, and the possibility to deeply modify the material depending on the fluorination conditions applied was presented. The first effect of fluorination is the compound delithiation to form a LiF shell around $FePO_4$ grains. If the temperature is increased, the iron phosphate matrix is converted little by little into α-FeF_3 which immediately reacts with the LiF layer to form α-Li_3FeF_6. When the temperature reaches 500°C the entire phosphate framework is consumed, and the material is completely converted into a mixture of FeF_3 and Li_3FeF_6. If the fluorinated phase is brought up to 550°C under an inert atmosphere as a second treatment, it is possible to obtain the $LiFePO_4F$ phase with an original methodology. The fluorinated phases demonstrated different electrochemical properties after 5 cycles depending on the fluorination

temperature. At 250°C, $FePO_4$ is surrounded by LiF possibly blocking the Li^+ pathway giving 45 $mAh.g^{-1}$ at 3.3V, whereas a mixture of FeF_3/Li_3FeF_6 is obtained at 500°C giving an important voltage hysteresis for the conversion reactions with 199 $mAh.g^{-1}$. After the second treatment under N_2 of $LiFePO_4$-125, the material shows a capacity of 55 $mAh.g^{-1}$ at 2.7V in agreement with the obtention of $LiFePO_4F$. This study is quite original because it is the first time that direct and total fluorination of $LiFePO_4$ under molecular F_2 have been reported, resulting in a solid/gas reaction extensible to other polyanionic compounds such as $Li_2FeP_2O_7$ or $Li_3Fe_2(PO_4)_3$,[42,43] but also $LiFePO_4(OH)$ which was already fluorinated but not by fluorine gas fluorination.[44] Nevertheless, the first electrochemical characterizations present limited performance and proves the necessity to carry out engineering of formulation on these materials to obtain better performance. Finally, in terms of perspective to this study, a cationic exchange with first the possibility to remove Li^+ by fluorination, and then the use of $FePO_4$ with a sodium anode was performed, resulting in $NaFePO_4$ with the triphylite structure which is electrochemically interesting as its lithium counterpart, and demonstrated a possible chemical delithiation to test any lithiated compound in another alkali ions batteries configuration.

Materials and methods

Synthesis

As starting material, we use a commercial nanostructurated LiFePO4, with triphylite structure. The nanosized grains (~150-200nm) are coated by a carbon layer ($LiFePO_4$/C : 2.5%wt). The material is purchased from "Phostech' lithium". Fluorinations are done by gas-solid treatments under pure fluorine gas in a nickel furnace. The furnace is connected to both fluorine and nitrogen bottles, and gases quantities coming from each bottle can be monitored. Two sets of experiments have been performed. Firstly, at "low temperatures" between room temperature (RT) and 350°C, and secondly at "high temperature" at 500°C. Fluorinations are done for 5h. A second treatment was done on some materials at 550°C under N_2 for 24h. All the fluorination treatments are summarized in Table S1. As a reference for Mössbauer spectrometry, α-Li_3FeF_6 with Fe_2O_3 as an impurity at 15 %Fe is obtained mixing Li_2CO_3 + $FePO_4.4H_2O$ in Hf_{aq} 48% with a second treatment under F_2 at 250°C.

Material characterization

Characterization methods

Powder X-Ray diffraction (PXRD): X-ray diffraction patterns were collected in the range $10° \leq 2\theta \leq 95°$ on a Panalytical MPD-PRO diffractometer equipped with a linear X'celerator detector with a CuK_α radiation (1.54 Å). A homemade measurement cell allowed the data to be collected under a static inert argon atmosphere. Data were collected in the [10-95°] 2θ scattering angle range with a 0.0836° step.

Mössbauer spectroscopy: Mössbauer spectroscopy has been measured on freshly prepared samples stored under argon. ^{57}Fe Mössbauer spectra were recorded in the constant acceleration mode and in transmission 20 geometry on a standard Mössbauer spectrometer composed of electronic devices from Ortec and Wissel. A ^{57}Co(Rh) source with a nominal activity of 370 MBq was used. The source and the absorber were always kept at room temperature. The thickness of the absorbers is about 10 mg/cm^2. The isomer shift is given relative to α-Fe standard at room temperature.

Transmission electron microscopy (TEM): Powder samples for TEM analysis are deposed on a copper grid with a carbon membrane by drop casting after dispersion in ethanol. Compounds were examined in CM20 Phillips transmission electron microscope (images were recorded at 200kV) and chemical analysis were done with an energy dispersive X-Ray spectroscope.

Fourier transformation infra-red spectroscopy (FTIR): Infrared spectra were collected, also during the defluorination step with a Nicolet Summit FTIR spectrometer (Thermo scientific) equipped with a heated MercuryTM gas cell (10 cm cell path, CaF_2 windows) coupled with the passivated nickel reactor. Spectra were recorded in the 1000 – 4000 cm^{-1} range with a 4 cm^{-1} resolution and 16 scans.

Electrochemical measurements: The electrochemical performances were investigated using galvanostatic cycling. The electrodes were composed of fluorinated sample (45% w/w), acetylene black (45% w/w) as conductive material and polyvinylidene difluoride (PVDF 10% w/w) as binder. After stirring in propylene carbonate (PC), the mixture was spread uniformly onto a stainless-steel current collector disk of 10 mm diameter. After the PC evaporation, the electrodes were dried in a vacuum oven at 120 °C overnight to remove traces of water and solvent before their transfer into an argon-filled glovebox. The anode was a lithium or sodium metal disk, and the separator was Celgard 2034. A two electrodes cell was used (Swagelok cell type), where lithium/sodium was both reference and counter electrodes. The electrolyte was 1.0 M $LiClO_4$ or $NaClO_4$ in propylene carbonate. The cells were assembled in an argon filled dried glove box. Relaxation was performed for at least 5 hours until the open circuit voltage (OCV) stabilization. Galvanostatic cycling, carried out on a VMP2-Z instrument from Biologic, were performed at room temperature by applying a constant current density of 5 mA/g in oxidation and 10 mA/g in reduction.

Raman Spectroscopy: A JOBIN YVON T64000 spectrometer with a charge-coupled device multichannel detector was used for Raman investigations at room temperature. The radiation source was a 514.5 nm argon laser line. The laser power was tuned to low power (100 mW) in order to avoid the sample decomposition under the beam. 3 scans of 640 s were made for a single spectrum. The resolution was equal to 0.08 cm^{-1}.

NMR: ^{19}F NMR measurements were carried out with a Bruker Advance Spectrometer with working frequency of 282.2, 300.0 and 78.8 MHz, respectively. A Magic Angle Spinning (MAS) probe

operating with 2.5 mm rotors was used allowing a 30 kHz spinning rate. A sequence with a single π/2 pulse duration of 4.0 μs was used. The chemical shifts were externally referenced to $CFCl_3$.

Conflicts of interest

There are no conflicts to declare.

Acknowledgements

All the authors want to thank Willmann Patrick[e] and the Centre National d'Etudes Spatiales (CNES), Hamwi André[a], Dubois Marc[a], Louvain Nicolas[a,d], Fonquernie Claire[a,b], El-Ghozzi Malika[a] for the fruitful discussions and technical supports during this work.

References

1 J. M. Tarascon and M. Armand, *Nature*, 2001, **414**, 359.
2 J. B. Goodenough and Y. Kim, *Chem. Mater.*, 2010, **22**, 587–603.
3 N. Nitta, F. Wu, J. T. Lee and G. Yushin, *Mater. Today*, 2015, **18**, 252–264.
4 K. Cao, T. Jin, L. Yang and L. Jiao, *Mater. Chem. Front.*, 2017, **1**, 2213–2242.
5 J. Cabana, L. Monconduit, D. Larcher and M. R. Palacín, *Adv. Mater.*, 2010, **22**, E170–E192.
6 A. K. Padhi, V. Manivannan and J. B. Goodenough, *J. Electrochem. Soc.*, 1998, **145**, 1518–1520.
7 Y. Yuan, Q. Wei, S. Yang, X. Zhang, M. Jia, J. Yuan and X. Yan, *Energy Storage Mater.*, 2022, **50**, 760–782.
8 Y. Kong, L. Yuan, Y. Liao, Y. Shao, S. Hao and Y. Huang, *Energy Mater.*, 2023, **3**.
9 P. Molaiyan, J. Valikangas, R. Sliz, D. D. Ramteke, T. Hu, A. Paolella, T. Fabritius and U. Lassi, *ChemElectroChem*, 2024.
10 H. Arai, S. Okada, Y. Sakurai and J. Yamaki, *J. Power Sources*, 1997, **68**, 716–719.
11 K. Lemoine, A. Hémon-Ribaud, M. Leblanc, J. Lhoste, J.-M. Tarascon and V. Maisonneuve, *Chem. Rev.*, 2022, **122**, 14405–14439.
12 F. Badway, F. Cosandey, N. Pereira and G. G. Amatucci, *J. Electrochem. Soc.*, 2003, **150**, A1209–A1218.
13 F. Badway, F. Cosandey, N. Pereira and G. G. Amatucci, *J. Electrochem. Soc.*, 2003, **150**, A1318.
14 P. Liao, J. Li and J. R. Dahn, *J. Electrochem. Soc.*, 2010, **157**, A355–A361.
15 A. Basa, E. Gonzalo, A. Kuhn and F. García-Alvarado, *J. Power Sources*, 2012, **197**, 260–266.
16 K. Lemoine, Y. Nagatani, J.-M. Grenèche and Y. Inaguma, *J. Phys. Chem. C*, 2022, **126**, 8248–8255.
17 M. Ati, M. T. Sougrati, N. Recham, P. Barpanda, J.-B. Leriche, M. Courty, M. Armand, J.-C. Jumas and J.-M. Tarascon, *J. Electrochem. Soc.*, 2010, **157**, A1007.
18 R. Tripathi, G. R. Gardiner, M. S. Islam and L. F. Nazar, *Chem. Mater.*, 2011, **23**, 2278–2284.
19 C. Masquelier and L. Croguennec, *Chem. Rev.*, 2013, **113**, 6552–6591.
20 D. Chen, G. Q. Shao, B. Li, G. G. Zhao, J. Li, J. H. Liu, Z. S. Gao and H. F. Zhang, *Electrochim. Acta*, 2014, **147**, 663–668.
21 H. Wang, J. Jiang, P. Y. Chen, Z. R. Wu, X. B. Niu, C. Y. Ouyang, J. Liu and L. P. Wang, *J. ENERGY Chem.*, 2024, **89**, 208–215.
22 Z. Pan, H. Chen, Y. Zeng, Y. Ding, X. Pu and Z. Chen, , DOI:10.20517/energymater.2023.61.
23 P. J. Dunn, J. D. Grice, D. E. Newbury, A. C. Roberts and W. L. Roberts, *Powder Diffr.*, 1988,

3, 93–95.
24 M. Leblanc, V. Maisonneuve and A. Tressaud, *Chem. Rev.*, 2015, **115**, 1191–1254.
25 R. Tripathi, G. Popov, B. L. Ellis, A. Huq and L. F. Nazar, *Energy Environ. Sci.*, 2012, **5**, 6238–6246.
26 N. Recham, J. N. Chotard, J. C. Jumas, L. Laffont, M. Armand and J. M. Tarasco, *Chem. Mater.*, 2010, **22**, 1142–1148.
27 M. Prabu, M. V Reddy, S. Selvasekarapandian, G. V. S. Rao and B. V. R. Chowdari, *Electrochim. Acta*, 2012, **85**, 572–578.
28 J. Jamnik and J. Maier, *Phys. Chem. Chem. Phys.*, 2003, **5**, 5215–5220.
29 A. S. Andersson, B. Kalska, L. Häggström and J. O. Thomas, *Solid State Ionics*, 2000, **130**, 41–52.
30 C. V Ramana, A. Mauger, F. Gendron, C. M. Julien and K. Zaghib, *J. Power Sources*, 2009, **187**, 555–564.
31 A. Tressaud, J. Portier, S. Shearer-Turrell, J.-L. Dupin and P. Hagenmuller, *J. Inorg. Nucl. Chem.*, 1970, **32**, 2179–2186.
32 M. Ménétrier, J. Bains, L. Croguennec, A. Flambard, E. Bekaert, C. Jordy, P. Biensan and C. Delmas, *J. Solid State Chem.*, 2008, **181**, 3303–3307.
33 L. Aldon, A. Perea, M. Womes, C. M. Ionica-Bousquet and J.-C. Jumas, *J. Solid State Chem.*, 2010, **183**, 218–222.
34 J. M. Grenèche and F. Varret, eds. G. J. Long and F. Grandjean, Springer US, Boston, MA, 1993, pp. 161–203.
35 N. Recham, J.-N. Chotard, L. Dupont, C. Delacourt, W. Walker, M. Armand and J.-M. Tarascon, *Nat. Mater.*, 2010, **9**, 68–74.
36 X. Hua, A. S. Eggeman, E. Castillo-Martínez, R. Robert, H. S. Geddes, Z. Lu, C. J. Pickard, W. Meng, K. M. Wiaderek, N. Pereira, G. G. Amatucci, P. A. Midgley, K. W. Chapman, U. Steiner, A. L. Goodwin and C. P. Grey, *Nat. Mater.*, 2021, **20**, 841–850.
37 C. Berlanga, I. Monterrubio, M. Armand, T. Rojo, M. Galceran and M. Casas-Cabanas, *ACS Sustain. Chem. Eng.*, 2020, **8**, 725–730.
38 Y. Xu, R. Dai, X. Wang, Z. Qiao, H. Wen, D. Ruan and Y. Wang, *Chem. Phys. Lett.*, 2024, **834**, 140983.
39 J. Kim, D.-H. Seo, H. Kim, I. Park, J.-K. Yoo, S.-K. Jung, Y.-U. Park, W. A. Goddard III and K. Kang, *Energy Environ. Sci.*, 2015, **8**, 540–545.
40 M. Lachal, R. Bouchet, A. Boulineau, S. Surblé, C. Rossignol, F. Alloin and S. Obbade, *Solid State Ionics*, 2017, **300**, 187–194.
41 F. Nozaki, S. Shomura, J. Hwang, K. Matsumoto and R. Hagiwara, *ACS Sustain. Chem. Eng.*, 2023, **11**, 1037–1043.
42 D. Riou, N. Nguyen, R. Benloucif and B. Raveau, *Mater. Res. Bull.*, 1990, **25**, 1363–1369.
43 A. S. Andersson, B. Kalska, P. Eyob, D. Aernout, L. Häggström and J. O. Thomas, *Solid State Ionics*, 2001, **140**, 63–70.
44 H. Yaghoobnejad Asl and A. Choudhury, *RSC Adv.*, 2014, **4**, 37691–37700.